Available online at www.sciencedirect.com
ScienceDirect
European Journal of Mechanics B/Fluids 26 (2007) 1–14

Transitional regimes and rotation effects in Rayleigh–Bénard convection in a slender cylindrical cell

P. Oresta [a], G. Stringano [b], R. Verzicco [b,*]

[a] *Politecnico di Bari, DIASS Viale del Turismo 8, 74100, Taranto, Italy*
[b] *Politecnico di Bari, DIMeG and CEMeC, Via Re David 200, 70125, Bari, Italy*

Received 7 April 2005; received in revised form 10 November 2005; accepted 20 April 2006

Available online 8 September 2006

Abstract

In this paper we analyze transitional regimes and mean flow structures for the thermally driven convective flow in a cylindrical cell of aspect-ratio (diameter over cell height) $\Gamma = 1/2$. The investigation is carried out through the numerical integration of the three-dimensional unsteady Navier–Stokes equations with the Boussinesq approximation. In particular the critical Rayleigh numbers for the onset of convection, for the unsteady, chaotic and turbulent regimes are computed for two values of the Prandtl number and comparisons with cylindrical cells of larger aspect-ratio are performed. The effect of the background rotation on the flow dynamics is also described showing that the heat transfer increase, already evidenced in the literature, is only obtained for a range of rotation rates. The rotation can enhance or inhibit the heat transfer and, at low Rayleigh numbers, it is a very effective way to inhibit vertical motions and to prevent horizontal thermal gradients. This is highly desirable in solidification and crystal growth processes where thermally induced motions cause material defects and crystal inhomogeneities.

Keywords: Thermal convection; Transitional regimes; DNS; Heat transfer; Rotation effects

1. Introduction

Thermal convection is the flow developing when a fluid layer, vertically confined by horizontal plates, is heated from below and cooled from above. The fluid thermal expansion, in fact, produces an unstable density gradient which, if strong enough, generates a flow motion [1,2]; depending on the fluid layer depth h, the temperature difference Δ and the fluid properties α, ν and k, respectively the thermal expansion coefficient, kinematic viscosity and thermal diffusivity, the resulting flow can be steady, unsteady, chaotic or turbulent. These regimes are mainly selected by two dimensionless control parameters the Rayleigh number $Ra = g\alpha\Delta h^3/(\nu k)$ and the Prandtl number $Pr = \nu/k$, g being the acceleration of gravity.

In the last decade, research in thermal convection has focused on the high Rayleigh number turbulent regime since it characterizes countless geophysical and industrial problems. In the literature there is a wealth of recent [3] and not so recent [4,5] theories which aim at explaining the flow behaviour in strongly turbulent conditions and this has

* Corresponding author. Tel.: +39 080 5963898; fax: +39 080 5963411.
E-mail address: verzicco@poliba.it (R. Verzicco).

0997-7546/$ – see front matter
doi:10.1016/j.euromechflu.2006.04.006

further oriented laboratory experiments in this direction. Among the various possibilities cylindrical cells of small aspect ratio Γ (cell diameter over height) have become very popular since their realization is relatively simple and, at the same time, they can cope without deforming with the hydrostatic forces exerted by the fluid on the side wall. This is particularly true for the recent cryogenic helium experiments where huge pressure changes are needed in order to obtain large Rayleigh number variations within the same set-up (see for example Chavanne et al. [6]).

To date the highest Rayleigh number experiments are those by Niemela et al. [7] and Chavanne et al. [6], respectively $Ra = 10^{17}$ and $Ra = 10^{14}$, both using cryogenic helium as working fluid ($Pr \simeq 0.7$) and a cylindrical cell of aspect-ratio $\Gamma = 1/2$. These experiments, in turn, have inspired the simulations by Verzicco and Camussi [8] and Amati et al. [9] that in the same geometry have reached $Ra = 2 \times 10^{11}$ and $Ra = 2 \times 10^{14}$. The numerical simulations have shown that around $Ra \approx 10^{10}$ the mean flow might undergo a transition and, even if before and after this transition the flow is fully turbulent several mean flow features are different; this mean flow instability was noticed by Wu and Libchaber [10] who refer that 'in the $\Gamma = 1/2$ cell the large-scale velocity switches direction from time to time' and recently confirmed also by the experiments of Roche et al. [11] who found a bimodal state for the mean flow. It should be stressed, however, that all the above experiments and numerical simulations were at $Pr = 0.7$ while recent experiments performed in the same geometry but in water ($Pr \simeq 5$) did not observe any transition and the mean flow consisted only of a stable single roll completely filling the cell [12].

The observed flow dynamics seem to suggest that, at least for a Prandtl number of the order of unity, the early turbulent stage, often referred to as 'soft turbulence' is affected by the previous regimes which unfortunately have not been studied in detail since experiments have mainly focused their attention on high Rayleigh number flows. One of the aims of this paper is therefore to fill this gap by a detailed numerical study of the flow regimes preceding turbulence. This is of particular importance when considering that the critical Rayleigh numbers for the onset of convection Ra_C, for the unsteady regime Ra_U and the transition to turbulence Ra_T depend also on the cell aspect ratio Γ and comparisons among different cell geometries are often performed in terms of Ra/Ra_C, Ra/Ra_U and Ra/Ra_T.

In this work we will consider also the effect of a background rotation (with the rotation vector aligned with the gravity) on the mean flow structure. This topic has been already covered by theoretical [13], experimental [14–18] and numerical [19] owing to its relevance to geophysical problems. A relevant common finding is that the effects of rotation produce an increase of the heat transfer through the Ekman pumping which forces vertical currents in the core of cyclonic vortex columns. We have shown, however, that this phenomenon might not be present at low Rayleigh numbers when rotation effects make the flow subcritical and convection is suppressed. The reason for performing this further analysis is that in some problems of solidification of melted materials the desired final geometry is a slender cylindrical sample and the presence of residual convective motion in the melted phase produces inhomogeneous temperature distributions which, in turn, cause material defects in the solid phase. We show in this paper that the background rotation can be an effective way to inhibit the vertical motion and to establish a purely vertical thermal stratification.

The paper is organized as follows: in the next section a description of the problem and of the numerical method is given while Section 3 contains the results. The flow without rotation is described in Subsection 3.1 while the effects of rotation are discussed in Section 3.2. The paper closes with some closing remarks and recommendations for future work.

2. The problem

The flow investigated in this paper is that developing in a cylindrical cell of aspect ratio $\Gamma = 1/2$ heated from below and cooled from above with an adiabatic side wall; all the cell surfaces are no–slip. The cell can rotate about the vertical axis with a constant angular velocity Ω and the flow arrangement is summarized in Fig. 1

The flow is solved by numerically integrating the three-dimensional unsteady Navier–Stokes equations with the Boussinesq approximation:

$$\begin{aligned} \frac{D\mathbf{u}}{Dt} &= -\nabla p + \theta\hat{x} + \left(\frac{Pr}{Ra}\right)^{1/2}\nabla^2\mathbf{u} - \frac{1}{Ro}\hat{x}\times\mathbf{u}, \qquad \nabla\cdot\mathbf{u} = 0, \\ \frac{D\theta}{Dt} &= \frac{1}{(PrRa)^{1/2}}\nabla^2\theta, \end{aligned} \tag{1}$$

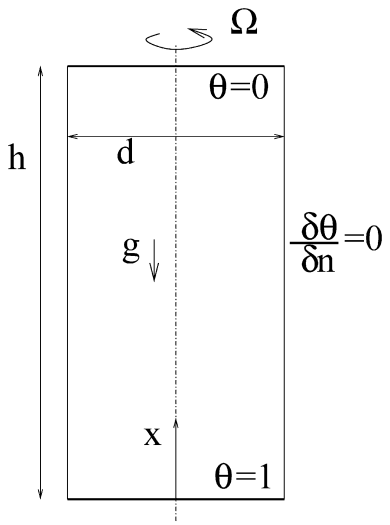

Fig. 1. Sketch of the cell.

with $\hat{x}$ the unity vector pointing in the opposite direction with respect to gravity, $\mathbf{u}$ the velocity vector, p the pressure (separated from its hydrostatic contribution), θ the non-dimensional temperature and $Ro = U/(2\Omega h)$ is the Rossby number with Ω the magnitude of the rotation vector anti-parallel to the gravity vector. The equations have been made non-dimensional using the free-fall velocity $U = \sqrt{g\alpha\Delta h}$, the distance between hot and cold plates h and their temperature difference $\Delta = T_h - T_c$, being T_h and T_c, respectively the temperatures of the lower hot and upper cold plates. The non-dimensional temperature θ is defined $\theta = (T - T_c)/\Delta$ and its range is $0 \leqslant \theta \leqslant 1$.

The equations have been written in a cylindrical coordinate frame and discretized on a staggered mesh by central second-order accurate finite-difference approximations; the resulting discretized system is solved by a fractional-step procedure with the elliptic equation inverted using trigonometric expansions in the azimuthal direction and a direct solver for the other two directions. The time advancement of the solution is obtained by a hybrid low-storage third-order Runge–Kutta scheme. The numerical method is the same as that described in Verzicco and Camussi [8] where further details of the numerical procedure can be found.

The computational domain has been discretized, depending on the Rayleigh and Prandtl numbers, with meshes containing up to $97 \times 49 \times 193$ gridpoints, respectively in the azimuthal, radial and vertical directions (the finest grid was used only for the simulations in the rotating regime at $Ra = 2 \times 10^8$ of Section 3.2). It is worth mentioning, however, that since most of the simulations of this paper are carried out at $Pr = 0.7$ and $Ra < 10^6$ the spatial resolution is not an issue; in fact, according to Belmonte, Tilgner and Libchaber [20] if the thickness of the thermal boundary layer is estimated as $\lambda_\theta \simeq h/(2Nu)$, with Nusselt numbers of the order of ten, it results $\lambda_\theta \simeq 5\%h$. Using a tanh-like stretching function as in Verzicco and Camussi [8] it is possible to cluster ten nodes within each thermal boundary layer while keeping the total number of nodes in the vertical direction below 80. In addition, since for this flow configuration the viscous boundary layer is thicker than the viscous one [8] the latter is even better resolved.

The non-dimensional time step size was dynamically adjusted in order to maintain the $CFL = \Delta t \max(|\mathbf{u}|/\delta)$ stability parameter below 1.2, $|\mathbf{u}|$ and δ are velocity magnitude and computational cell size. Note that this threshold is largely conservative since the low-storage third order Runge–Kutta integration scheme is stable up to $CFL = \sqrt{3}$ and, with the help of the viscous terms, simulations at $CFL = 2$ are easily run. Regardless the stability limit the time step size was kept always below $\Delta t = 0.02$ so that a minimum of a hundred time steps were needed to advance one large-eddy turnover time ($\approx 2h/U$). It is worth mentioning that immediately after the onset of convection a large scale flow is produced therefore the concept of large-eddy turnover time can be applied also for the transitional regimes. Nevertheless even when the mean flow breaks into smaller structures the large-eddy turnover time still is the longest convective time scale that can be supported by the flow thus yielding a conservative estimate of the slowest phenomena.

Both the spatial discretization and the time-step size have been verified against the criteria given by Grötzbach [21] and the numerical simulations by Verzicco and Camussi [8]. More in particular the above grid, combined with a non-

uniform mesh in the radial and vertical directions, assured that a minimum of 8 nodes were clustered within each thermal boundary layer while the viscous boundary layer, being thicker, was even more resolved. As a further check the case at $Pr = 0.7$ and $Ra = 9 \times 10^5$ initially run on a grid with $49 \times 33 \times 129$ points has been repeated using $65 \times 49 \times 193$ points obtaining, respectively, $Nu = 9.20 \pm 0.18$ and $Nu = 9.24 \pm 0.23$ with the first and the second grid; this is not surprising upon considering that the grid $65 \times 49 \times 193$ has more points than that used by Verzicco and Camussi [8] for the computation of the flow at $Ra = 2 \times 10^6$.

Every simulation has been started from rest in order to avoid hysteresis phenomena which are common in the chaotic regimes; in particular all the velocity components were set equal to zero and over a linear (purely conductive) temperature profile it was superimposed a random perturbation of maximum amplitude $\Delta\theta_{\text{random}} = 0.02$.

One of the main quantities used to monitor the flow dynamics is the Nusselt number which is the heat flux transferred between the plates normalized by its purely conductive value (the value in absence of fluid motion). In non-dimensional variables one can write $Nu = 1 + \sqrt{Ra\,Pr}\langle u_x\theta\rangle$ [22] where the angular brackets indicate average over time and over the whole fluid layer. The Nusselt number can also be evaluated by computing directly the mean heat flux at the hot and cold plates $Nu = \overline{\partial\theta/\partial x}|_w$ where $|_w$ indicates that the derivative is evaluated at the wall and the overbar implies an average in time and over the plate surface. The latter definition requires an adequate spatial resolution of the thermal boundary layer while the former expression needs a correct estimation of the fluctuations in the bulk in order to evaluate the correlation $u_x\theta$. The comparison of the Nusselt numbers obtained by different definitions can therefore be used as a cross check for the adequacy of the resolution close to the plates and in the bulk.

3. Results

3.1. Flow without background rotation

Following Rayleigh [2] the flow starts moving owing to buoyancy only if the Rayleigh number exceeds a threshold value known as critical Rayleigh number Ra_C. This parameter is independent of the Prandtl number but depends on the cell aspect-ratio Γ, on its shape (cubic, cylindrical, etc.) and on the wall boundary conditions (no-slip or free-slip for the velocity, constant temperature or constant heat flux for the temperature). Linear stability analyses have been performed for any combination of boundary conditions for horizontally infinite domains (see [13]) while less is known for the confined configurations and in particular for cylindrical geometries. Further, for cylindrical cells there is the additional issue of identifying the most unstable mean flow structure since despite the axisymmetric geometry the large-scale flow might not have the same symmetry. This is the case of the cylindrical $\Gamma = 1$ cell and, as shown by Verzicco and Camussi [23] if the flow axial symmetry is enforced the onset of convection can be delayed up to $Ra = 11300$ in contrast to $Ra_C = 3750$ that is the critical Rayleigh number for the full three-dimensional flow.

Following that paper in the present study the flow was left free to develop three-dimensional structures and the value of Ra_C has been obtained from the neutral stability of the most unstable kinetic energy azimuthal Fourier mode. Namely, given the cylindrical geometry it is possible to decompose the velocity field $\mathbf{u}(r, \theta, z, t)$ into azimuthal Fourier modes $\hat{\mathbf{u}}(r, n, x, t)$ which, after integration in the meridional $r - x$ plane yield the azimuthal kinetic energy mode

$$E_n(t) = \pi \int_0^R \int_0^h \hat{\mathbf{u}}(r, n, x, t)\hat{\mathbf{u}}^*(r, n, x, t)\,\mathrm{d}r\,\mathrm{d}x$$

($\hat{\mathbf{u}}^*$ is the complex conjugate of $\hat{\mathbf{u}}$). A plot of the time evolution for these modes is given in Fig. 2(a) where it is evident that in the $\Gamma = 1/2$ cell the $n = 1$ mode is the most unstable, it grows exponentially until saturation and the other modes, including the axisymmetric $n = 0$, grow only afterward owing to non-linear interaction.

Depending on the Rayleigh number the $n = 1$ mode growth rate is positive ($Ra > Ra_C$) or negative ($Ra < Ra_C$) and in the latter case any fluid motion is damped. The value of Ra which gives a neutral $n = 1$ mode gives the critical Rayleigh number and according to Fig. 2(b) it results $Ra_C = 2.35 \times 10^4$. Note that the value of Ra_C was obtained from Fig. 2(b) by linearly interpolating on the growth rates of the most unstable ($n = 1$) mode. This value is in reasonable agreement with Charlson and Sani [24] which by a linear stability analysis predict $Ra_C \simeq 25\,000$. An additional result of that analysis is that for the aspect ratio $\Gamma = 1/2$ the most unstable structure is not axisymmetric but it rather consists of a single roll, completely filling the cell. The theory further predicts that the single large roll shows up at the onset

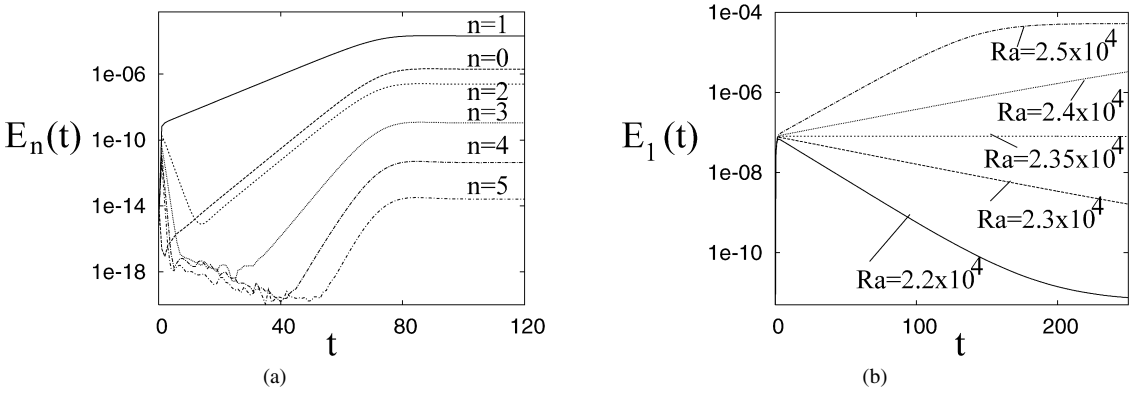

Fig. 2. Time evolution of kinetic energy azimuthal modes for the $\Gamma = 1/2$ cell at $Pr = 0.7$: (a) modes from $n = 0$ to $n = 5$ at $Ra = 3 \times 10^4$, (b) mode $n = 1$ at different Rayleigh numbers.

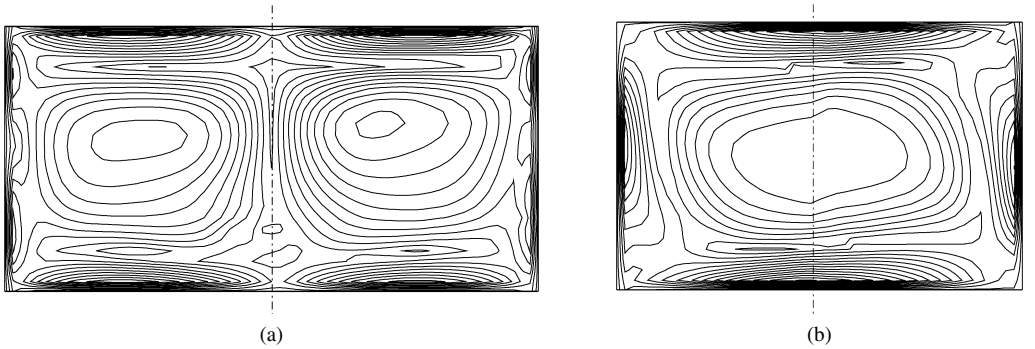

Fig. 3. Vorticity magnitude in the meridional planes $\theta = 0$ and $\theta = \pi/2$ at $Ra/Ra_C = 1.025$ and $Pr = 0.7$; (a) $\Gamma = 2$, (b) $\Gamma = 1.5$. ($\Delta\omega = 0.2$.)

of convection in cylindrical cells up to $\Gamma \leqslant 1.62$ and only for larger aspect ratios the onset of convection produces an axisymmetric flow.

This has been verified by direct numerical inspection as shown in Fig. 3. In particular, numerical simulations have been performed at the fixed ratio $Ra/Ra_C = 1.025$ for several aspect ratios Γ indeed obtaining a single large roll for $\Gamma < 1.6$ and an axisymmetric flow for larger cells. It should be stressed, however, that even in the largest cell ($\Gamma = 2$) if the single roll is initially enforced by ad hoc perturbations this is sustained in the developed flow. In addition, at least for $\Gamma \leqslant 2$, regardless of the initial conditions, a single large structure always emerged for ratios Ra/Ra_C large enough to produce an unsteady flow.

We note, on the side, that in many papers the critical Rayleigh number is defined as the value at which the Nusselt number departs from the purely conductive value $Nu = 1$. At the onset of convection, however, the difference $Nu - 1$ is proportional to $Ra - Ra_C$ and the former vanishes as Ra approaches Ra_C; this makes difficult to distinguish, when $Ra \to Ra_C$, a truly deviation of the Nusselt number from unity and unavoidable round-off errors. In contrast, the growth rate of the most unstable mode $n = 1$, around Ra_C, switches sign from negative to positive values and the zero-crossing makes the identification of the critical value unambiguous.

As the Rayleigh number is augmented with respect to the critical value the flow maintains steady with the Nusselt number progressively departing from unity and the flow velocity increasing as $(Ra - Ra_C)^{1/2}$. This velocity increase, in turn, causes the increase of the non-linear terms that eventually exceed the viscous ones thus leading to the flow unsteadiness [25]. The transition from the steady to the unsteady regime identifies another critical Rayleigh number Ra_U which can be defined as the minimum value of Ra for the flow to develop non-decaying oscillations. The value of Ra_U, however, depends on the Prandtl number and the reason is easily understood upon considering that the flow Reynolds number is proportional to $(Ra/Pr)^{1/2}$ (see Eq. (1)). If the onset of unsteady flows is given by the balance between viscous and convective terms the Reynolds number must be clearly the control parameter and the smaller the Prandtl number the smaller the Ra_U at which the unsteady transition occurs. In Fig. 5 the time evolution of the energy

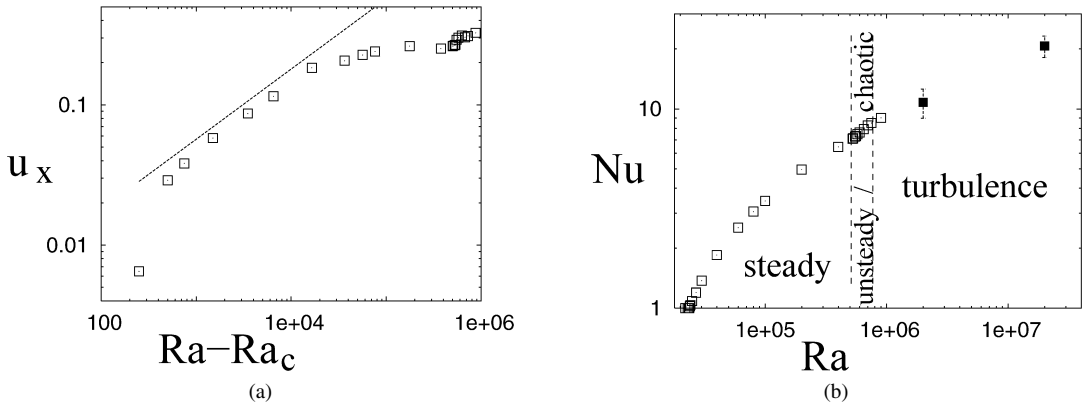

Fig. 4. (a) Maximum vertical velocity u_x vs $Ra - Ra_C$ at $Pr = 0.7$ (the dashed line is the $1/2$ slope). (b) Nusselt number vs Rayleigh number at $Pr = 0.7$ (the last two turbulent values ■ are from Verzicco and Camussi [8]).

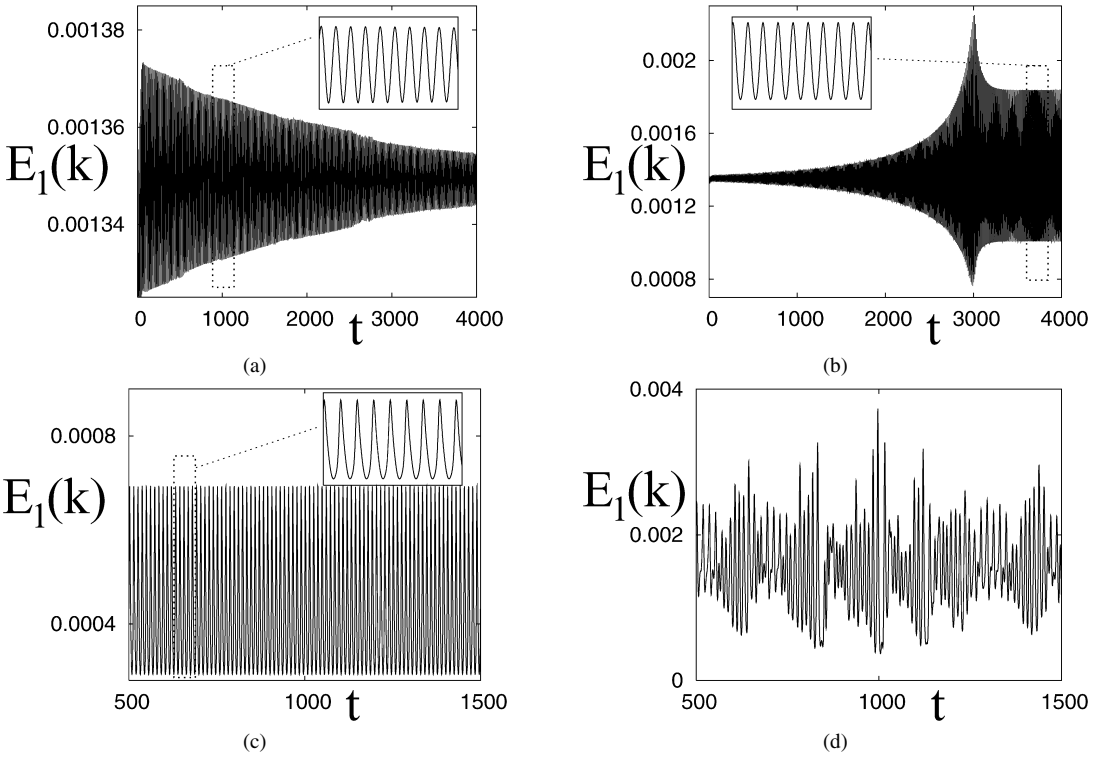

Fig. 5. Time history of $E_1(t)$ at $Pr = 0.7$ and different Rayleigh numbers: (a) $Ra = 5.5 \times 10^5$, (b) $Ra = 5.6 \times 10^5$, (c) $Ra = 6.5 \times 10^5$, (d) $Ra = 7.5 \times 10^5$.

mode $E_1(t)$ is reported at $Pr = 0.7$ showing different flow behaviours for increasing Rayleigh numbers. It is worth noting that the identification of Ra_U is more involved than Ra_C since the presence of an oscillatory flow behaviour alone does not guarantee the onset of the time periodic regime. In fact at $t = 0$ the fluid is at rest and a perturbation is applied on the temperature field; since this is not a stable configuration the flow relaxes to a proper equilibrium state according to its own dynamics. If the Rayleigh number is $Ra_C < Ra < Ra_U$ the relaxation can occur with oscillations even if the asymptotic state is steady; the relaxation time is longer the closer Ra is to Ra_U implying that around Ra_U simulations must be carried out for thousands of large-eddy-turnover times in order to be able to distinguish between slowly damped from sustained oscillations.

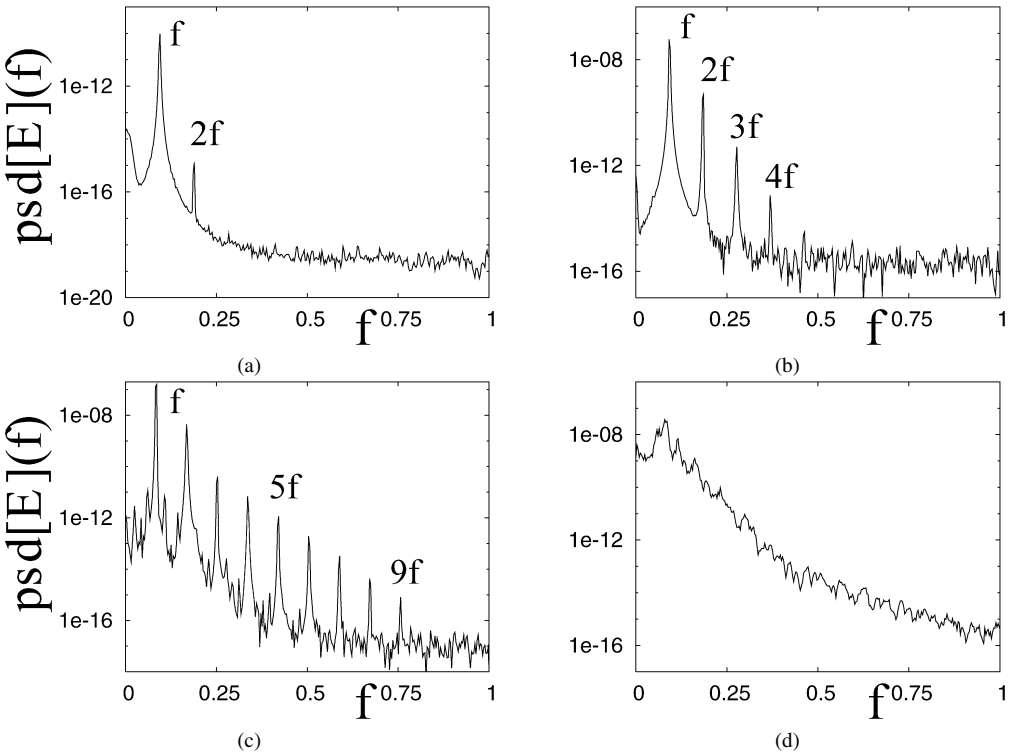

Fig. 6. The same as Fig. 5 for the frequency spectrum of $E_1(t)$.

This is certainly the case of Fig. 5(a) showing the time history of $E_1(t)$ at $Ra = 5.5 \times 10^5$; when observed on a short time window (order of 100 time units) the flow seems to oscillate sinusoidally while in the long term the oscillations decay exponentially. We wish to stress that this behaviour cannot be ascribed to an initial transient since the duration of the simulation is considerably longer than any diffusion time that, based on the kinematic viscosity ν or the thermal diffusivity k is, respectively, $T_\nu = \sqrt{Ra/Pr} \simeq 886$ or $T_k = \sqrt{Ra\,Pr} \simeq 620$ time units. This implies that the continuous decreasing amplitude of the oscillations is the secular trend of the flow that eventually will attain a steady state. The case at $Ra = 5.6 \times 10^5$ displays a different behaviour since it has an initial transient with the oscillation amplitude diverging exponentially until saturation followed by a periodic oscillation with constant amplitude. This could be assumed as the beginning of the unsteady regime although it could be argued that in between $Ra = 5.5 \times 10^5$ and 5.6×10^5 there is a Rayleigh number at which the flow oscillates since the beginning of the evolution which can be thought of as either a limiting case of vanishing damping (Fig. 5(a)) or vanishing amplification (Fig. 5(b)). Although the precise pinpointing of Ra_U would be possible by carrying out additional time consuming numerical simulation, this would be a result with little practical interest since, on account of the 1.8% difference between $Ra = 5.5 \times 10^5$ and 5.6×10^5, it is unlikely that such an 'exact' value would be reproduced by any other experiment or simulation.

Figs. 6(a), (b) show the spectra of the signals of Figs. 5(a), (b) (the latter is computed only over the constant amplitude time window while the former over the whole time extent. This produces a low frequency component which is evident at the origin $f = 0$) where it is evident that already at $Ra = 5.6 \times 10^5$ the signal does not contain a single frequency. In fact the spectrum evidences the main harmonic with three additional peaks whose frequency is an integer multiple of the main one. In agreement with Verzicco and Camussi [23] the main peak frequency is produced by the meridional oscillation of the large scale recirculation while the harmonics are due to the azimuthal tilting of the same structure.

As the Rayleigh number is further increased additional high frequency peaks develop (Fig. 6(c)) and their non-linear interaction, in turn, produces further peaks which become denser in the frequency space and eventually lead to a continuous spectrum. As shown in Fig. 6(d) this is already evident at $Ra = 7.5 \times 10^5$ although it is only for $9 \times 10^5 \leqslant Ra \leqslant 10^6$ that not only the temporal evolution but also the spatial distribution of the flow scales indicates the beginning of the transition to turbulence. Indirect evidence of this regime is given by Fig. 4(b) showing that,

starting from $Ra_T \approx 10^6$ the Nu vs Ra relation follows a power law. Indeed Fig. 4(b) shows only two points within the turbulent regime and it might be questionable if beyond Ra_T the Nusselt number really follows a power law. It must be noted, however, that the Nu values for $Ra > 10^6$ are the data from Verzicco and Camussi [8] were simulations are conducted up to $Ra = 2 \times 10^{11}$ and power laws can be estimated without uncertainties.

It is worth mentioning that the dynamics evidenced by Figs. 5 and 6 have several analogies and differences with the scenario proposed by Verzicco and Camussi [26] for the $\Gamma = 1$ cylindrical cell. In particular, in that wider cell the onset of the unsteady regime was characterized by a pure single-frequency oscillation and the transition to chaos occurred following the period doubling mechanism with the generation of the multiple frequencies $(2f, 3f, \ldots)$ accompanied by the sub-harmonics $(f/2, 3f/2, \ldots)$. In the present $\Gamma = 1/2$ cell, in contrast, the onset of the unsteady convection is already characterized by multiple frequency oscillations and the spectra are progressively filled only by multiple harmonics produced via non-linear interactions without evidence of sub-harmonics up to the transition to turbulence. Considering that the non-linear interaction between the frequencies m and n leads to the frequencies $(m+n)/2$ and $(m-n)/2$ the absence of sub-harmonics in the spectra of Fig. 6 clearly indicates that the steady component of the flow (the part with zero-frequency) is too weak to interact non-linearly with any other frequency. This is better understood upon considering that the equation for the evolution of the amplitude $A_{(m+n)/2}$ of the mode with frequency $(m+n)/2$ has a source term $A_m A_n$ in which, if $(m+n)/2$ is a subharmonic of m or n, either m or n are zero. The absence of any sub-harmonic in the spectra of Fig. 6 can therefore be taken as an indication of the negligible value of the source term $A_m A_n$ which in turn implies the vanishing nature of the zero frequency (time constant) mode of amplitude A_0.

A similar analysis as that of Figs. 5 and 6 has been performed for the same geometry but at $Pr = 0.022$ instead of $Pr = 0.7$. We have observed the same dynamics as at $Pr = 0.7$ even if, consistently with the role of the Prandtl number, we have found $Ra_U = 4.5 \times 10^4$ and $Ra_T \approx 7.5 \times 10^4$ at $Pr = 0.022$ (to be compared with $Ra_U = 5.6 \times 10^5$ and $Ra_T \approx 10^6$ at $Pr = 0.7$).

Additional important differences between the $\Gamma = 1$ and the present $\Gamma = 0.5$ cylindrical cell is in the mean flow dynamics that has recently gained interest owing to questions related to 'wind reversals'. In particular, it has been observed (see [27] among many others) that in the $\Gamma = 1$ cell, superimposed to the background turbulence, there is a large-scale recirculating motion often referred to as 'mean wind'. This wind sweeps the horizontal plates producing viscous and thermal boundary layers and therefore influencing the heat transfer. The experimental evidence is that this large-scale roll is generated since the onset of convection and it persists at least for several decades of Ra and Pr; the roll maintains a fixed orientation for hundreds of large-eddy-turnover times although, if the Rayleigh number is large enough, it experiences sudden irregular reversals, in a time of the order of one large-eddy-turnover time, whose statistics were analyzed in detail by Sreenivasan, Bershadskii and Niemela [28]. The same study, however also showed that at $Pr = 0.7$ the 'reversal factor' γ (the ratio of the time the wind is in one direction over the time it is in the opposite direction) was of the order of unity only at $Ra \approx 10^{11}$ while at $Ra \approx 10^8$ it was $\gamma \approx 100$; this implies that for the low values of the Rayleigh number ($< 10^6$) analyzed in the present study wind reversals should not be observed. This was indeed verified by running few numerical simulation in a $\Gamma = 1$ cylindrical cell at $Pr = 0.7$ and $Ra \leqslant 3 \times 10^5 = 80 Ra_C$ and monitoring the time history of the vertical velocity signal sampled over diametrical opposite positions. A typical record is given in Fig. 7(a) with the structure of the mean flow in vertical and horizontal cross sections in Fig. 8.

The same analysis carried out on the $\Gamma = 0.5$ cell gave the unexpected result of Fig. 7(b) already at $Ra = 9 \times 10^5 = 38.2 Ra_C$ showing reversal-like velocity histories. Taking advantage of the data accessibility of the numerical simulation we were able to investigate the three-dimensional flow structure during one reversal-like event in order to understand the real flow dynamics. Some results are shown in Figs. 9–11 where it is evident that more than a reversal of the large scale roll is a temporary break-up of the large recirculation into two unity aspect-ratio rolls that immediately merge to reform a single structure with a different orientation. This result is particularly interesting since Verzicco and Camussi [8] who analyzed the same configuration at $2 \times 10^6 \leqslant Ra \leqslant 2 \times 10^{11}$ observed that the dominant structure of the mean flow was a singe large scale roll for $Ra < 10^{10}$ and two unity aspect ratio rolls otherwise. In that case, however the large computational time required by the high Rayleigh number cases did not allow for a long time integration and it was not clear therefore if the observed mean flow configurations were the only stable structures or if rather there were two possible states whose relative probability changed with the Rayleigh number. According to the present numerical evidence and the papers by Roche et al. [11] and Verzicco and Camussi [8] the second scenario seems more likely to occur. In particular, the two possible mean flow structures are a single slender recirculation completely filling the cell or two counter-rotating unity aspect ratio rolls; for $Pr = 0.7$ the first status is the most probable

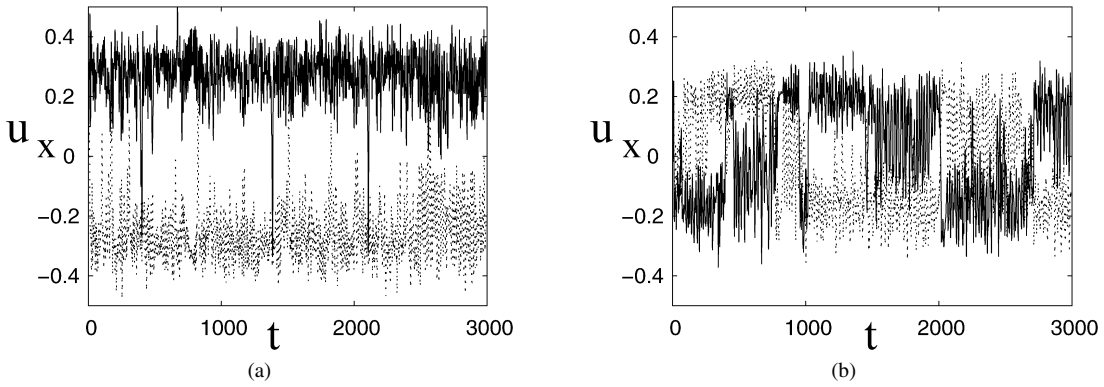

Fig. 7. Time histories of pointwise samples of vertical velocity. ——- and - - - - lines are for diametrically opposite sampling points. (a) $\Gamma = 1$, $Ra = 3 \times 10^5$ and $Pr = 0.7$, probes at $x/h = 0.5$ and $r/h = 0.4$. (b) $\Gamma = 0.5$, $Ra = 9 \times 10^5$ and $Pr = 0.7$, probes at $x/h = 0.25$ and $r/h = 0.2$.

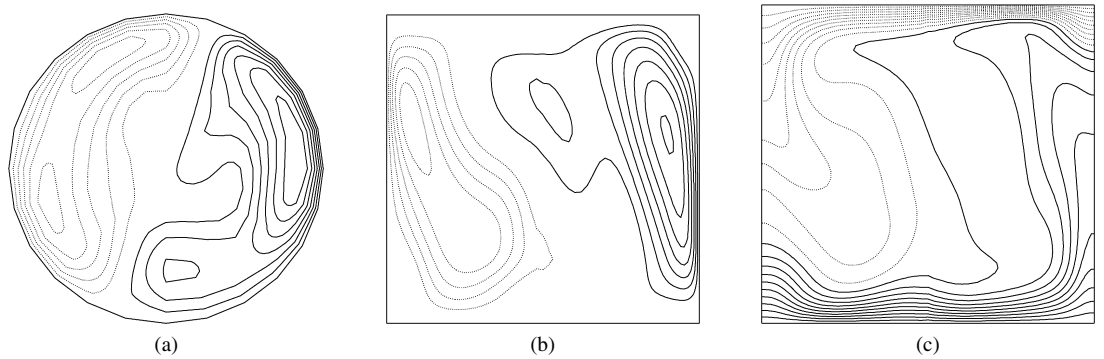

Fig. 8. Instantaneous horizontal and vertical sections of vertical velocity and temperature at $Ra = 3 \times 10^5$ and $Pr = 0.7$ in the $\Gamma = 1$ cell. (a) Horizontal section of vertical velocity halfway between the plates ——- positive, - - - - negative values. $\Delta u = \pm 0.05$. (b) Vertical section of vertical velocity, contours as in (a). (c) Vertical section of temperature - - - - $0 \leqslant \theta < 0.5$, —— $0.5 < \theta \leqslant 1$ thick ——- fort $\theta = 0.5$. ($\Delta\theta = 0.05$.)

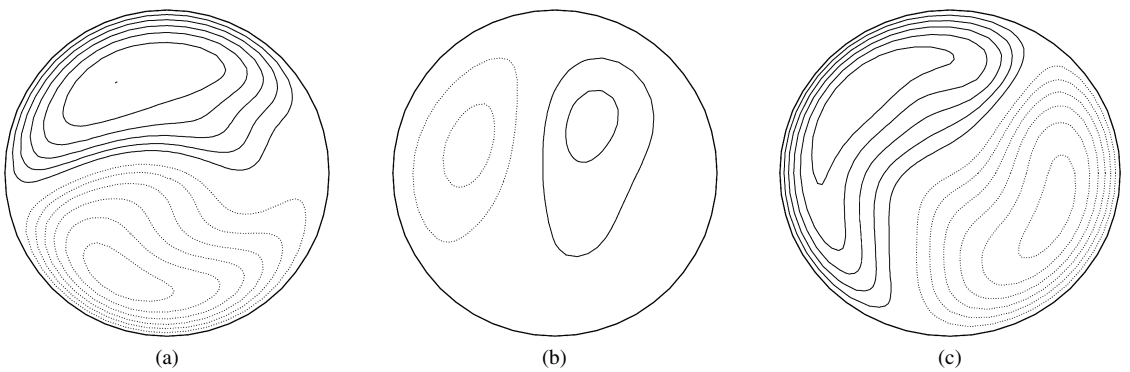

Fig. 9. Instantaneous horizontal sections of vertical velocity halfway between the plates at $Ra = 9 \times 10^5$, $Pr = 0.7$ and $\Gamma = 1/2$: (a) $t = 1700$, (b) $t = 1800$, (c) $t = 1900$. ——- positive, - - - - negative values. ($\Delta u = \pm 0.05$.)

at $Ra \leqslant 10^{10}$ while the second prevails at larger Rayleigh numbers. For $Ra \simeq \mathcal{O}(10^{10})$ the two structures have similar probability to occur and this brings to the bimodal status and the scattering of the measurements evidenced by Roche et al. [11]. The mean flow break-up from a single recirculation into two counter-rotating unity aspect ratio cells was recently investigated by Stringano and Verzicco [29]; they found that these transitions are a peculiarity of the $\Gamma = 1/2$ cell and can be explained by comparing the different time scales of the plumes and large scale flow depending on Ra and Pr.

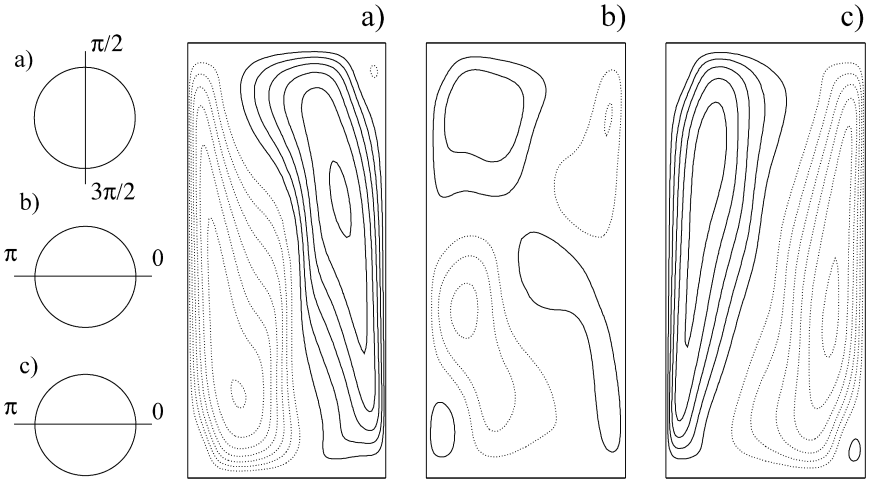

Fig. 10. The same as Fig. 9 for vertical meridional sections. $Ra = 9 \times 10^5$, $Pr = 0.7$ and $\Gamma = 1/2$.

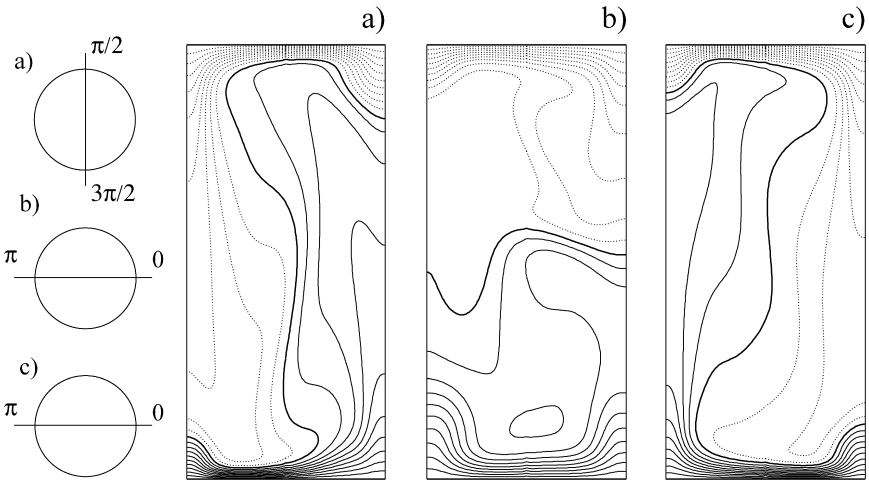

Fig. 11. The same as Fig. 10 for temperature: - - - - $0 \leqslant \theta < 0.5$, —— $0.5 < \theta \leqslant 1$ thick —— fort $\theta = 0.5$. ($\Delta\theta = 0.05$.)

3.2. Flow with background rotation

In this section we want to describe the changes produced in the flow dynamics by a background rotation. According to Eqs. (1) an additional control parameter, the Rossby number *Ro*, comes into play and this alters the scenario described in the previous section. The new emerging dynamics is better understood if one recalls the Taylor–Proudman theorem stating that in a fluid rotating around the vector $\Omega\mathbf{k}$, if the rotation is *fast enough*, it results $\mathbf{k} \cdot \nabla\mathbf{u} = 0$ or $\partial u_i/\partial k = 0$ [30]. It implies that if the rotation is dominant with respect to a typical flow velocity, in other words if the Rossby number $Ro = U/(2\Omega h)$ is small, the rotation counters the velocity gradients in the direction of the rotation vector and any variation in that direction tends to be suppressed. Note however that this does not necessarily imply that the flow must remain two-dimensional because even if the gradients along k are inhibited a constant velocity aligned with the rotation vector is allowed by the Taylor–Proudman theorem. Constant ascending and descending currents have in fact been observed within the core of columnar vortices that organize themselves cyclonically on account of the conservation of angular momentum (when the fluid is radially drained into the columns at the horizontal boundaries) [17–19]. These currents reconnect at the horizontal hot and cold plates within the Ekman layer that, via its pumping, forces the vertical motions. There is general agreement on the efficiency of this mechanism in extracting heat from the plates and the overall effect is a slight increase of the Nusselt number observed by Rossby [14] and confirmed

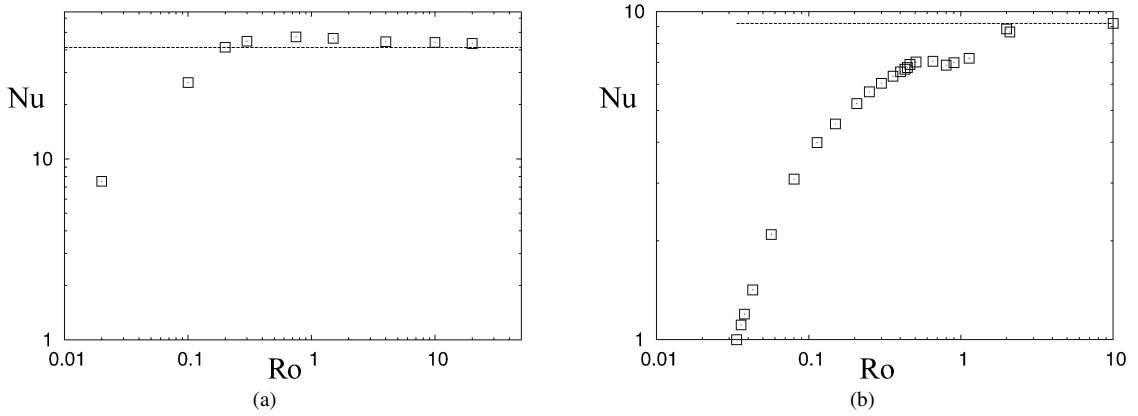

Fig. 12. Nusselt number versus Rossby number at $Pr = 0.7$ in a $\Gamma = 1/2$ cell. (a) $Ra = 2 \times 10^8$, (b) $Ra = 9 \times 10^5$. The dashed lines are, respectively, $Nu = 41.32$ and $Nu = 9.2$ in figures (a) and (b) which are the Nusselt numbers obtained without rotation ($Ro \to \infty$).

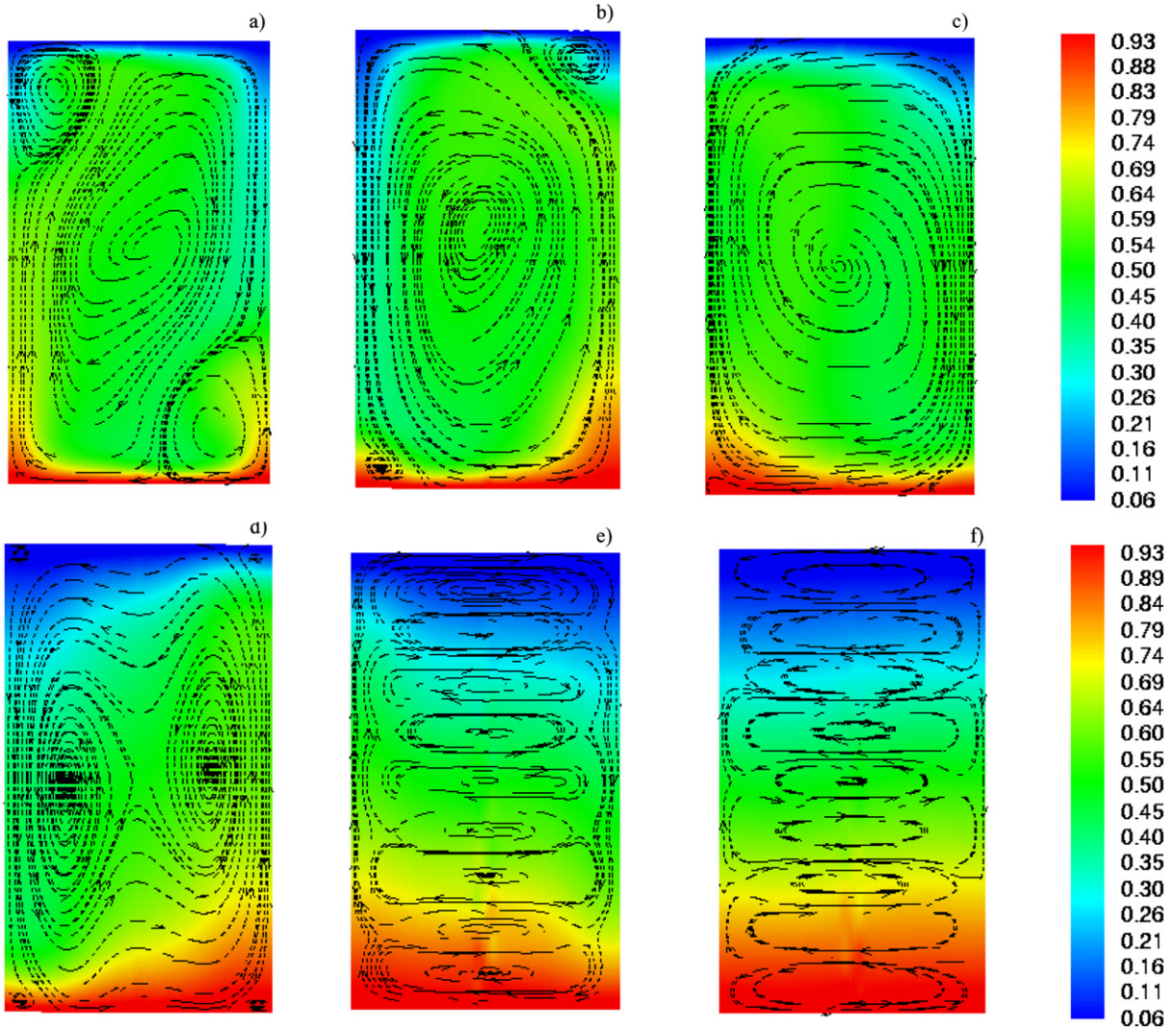

Fig. 13. Vertical cross sections of temperature with streamlines in the $\Gamma = 1/2$ cell at $Pr = 0.7$ and $Ra = 9 \times 10^5$: (a) $Ro = 2$, (b) $Ro = 0.463$, (c) $Ro = 0.15$, (d) $Ro = 0.08$, (e) $Ro = 0.043$ and (f) $Ro = 0.036$.

by many other studies (see for example [31,32]. This phenomenon has been observed also in the present paper by numerical simulations at $Ra = 2 \times 10^8$, $Pr = 0.7$ over a wide range of Rossby numbers. In particular Fig. 12(a) shows that the heat transfer is increased by about 15% in agreement with similar studies. Fig. 12(a), however, shows also that as the Rossby number attains very small values (very high rotation rates) the Nusselt number decreases with respect to its value without background rotation.

The reason for the heat transfer decrease can be understood when considering that according to the linear stability analysis by Chandrasekar [13] the critical Rayleigh number for the onset of convection increases as $Ra_C \sim Ta^{2/3}$ being $Ta = 4\Omega^2 h^4/\nu^2$ the Taylor number. From the definitions of Ra, Pr and Ro we have $Ta = Ra/(Pr\,Ro^2)$ and the above stability relation can be written as

$$\frac{Ra}{Ra_C} \sim Pr^{2/3}\, Ra^{1/3}\, Ro^{4/3}. \tag{2}$$

This implies that for fixed Rayleigh and Prandtl numbers, as the Rossby number decreases the ratio Ra/Ra_C decreases as well and it can become too small to sustain the same flow regime as in absence of rotation.

Eq. (2) suggests also that for a given Ro the value of Ra/Ra_C decreases with Ra and for a given combination of small Rayleigh and Rossby numbers the flow can become subcritical. This is exactly the case of Fig. 12(b) where the flow has been computed at $Ra = 9 \times 10^5$; in this case a decrease of the Rossby number produces a continuous decrease of the heat transfer up to a purely conductive value in which any flow motion is suppressed.

More in detail, the analysis of the flow time dependence shows a behaviour similar to that of Fig. 4(b) with the Rossby number taking the role of the Rayleigh number, even if the curve of Fig. 12(b) shows some irregularities presumably due to the changes in the mean flow structure produced by rotation (see Fig. 13). In particular, since for increasing rotation rates the vertical velocity is progressively reduced, an initially turbulent-like flow becomes chaotic, multi-periodic and steady. Finally at the highest rotation rates the flow suppression is complete and the Nusselt number recovers the purely conductive value.

The above described scenario is confirmed by Figs. 13 where vertical sections of the mean flow are reported. It is interesting to note that as the recirculation is slowed down by rotation effects the horizontal inhomogeneity of the temperature field becomes less pronounced and, when the large scale roll is suppressed the temperature field attains a conductive structure with only a vertical gradient and without horizontal temperature differences. The panels of Fig. 13 are mainly intended to show how the mean flow structure and consequently the temperature field are modified by the effects of rotation. Further details on the single velocity components can be obtained from the sections as in Fig. 14 where the case of Fig. 13(d) is shown more in detail. Apart from the particular shape of the recirculation which is essentially determined by the Rossby number the relevant difference between Fig. 14 and Figs. 7–11 is the peak value of each velocity component that in the rotating case never exceeds the value $0.01U$ in contrast to the peaks of the order of $0.3-0.5U$ for the non-rotating cases. The conditions of negligible residual motions and uniform horizontal temperature is highly desirable in solidification processes where horizontal temperature gradients can cause residual thermal stresses in the material and defects in the crystal growth [33].

4. Conclusions

Numerical simulations of the thermally driven flow at $Ra < 10^6$ have been employed to analyze the different flow regimes developing from the onset of convection up to turbulence. This range of small Rayleigh numbers is usually inaccessible to the nowadays experimental set-ups which are designed to cover the high Rayleigh number regime [11,7]. The results have shown that since the onset of convection, occurring at $Ra = 2.35 \times 10^4$, a mean flow develops consisting of a single recirculation completely filling the cell. For increasing Rayleigh numbers (respectively $Ra = 4.5 \times 10^4$ at $Pr = 0.022$ and $Ra = 5.6 \times 10^5$ at $Pr = 0.7$) the flow becomes unsteady and as the Rayleigh number is further increased multiple frequencies are introduced in the spectra of the velocity signals until the spectrum becomes continuous thus indicating the onset of the turbulence. This occurs at $Ra \approx 7.5 \times 10^4$ at $Pr = 0.022$ and $Ra \approx 10^6$ at $Pr = 0.7$ consistently with the role of the Prandtl number.

A similar dynamics was observed by Verzicco and Camussi [23] for a cylindrical cell of aspect ratio $\Gamma = 1$ although in that case the beginning of the unsteady regime was characterized by a single frequency in the spectra while in the present slender cell multiple frequencies are observed since the beginning of the unsteady dynamics. A significant difference between the two geometries is the dynamics of the mean flow that in the $\Gamma = 1$ remains stable while in the

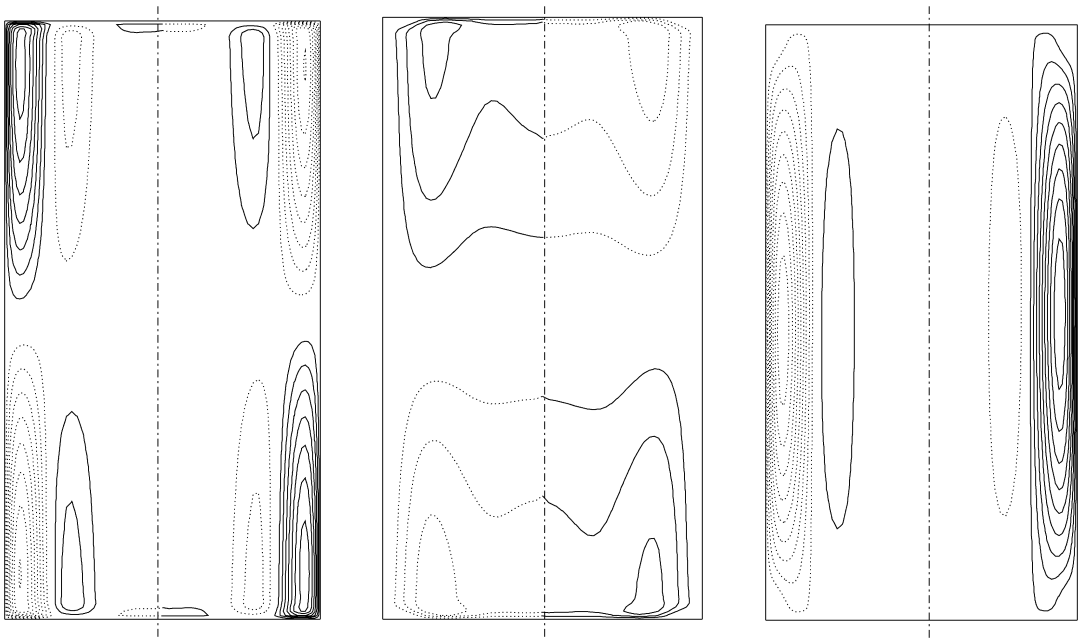

Fig. 14. Contour lines of velocity components over a vertical cross section in the $\Gamma = 1/2$ cell at $Pr = 0.7$, $Ra = 9 \times 10^5$ and $Ro = 0.08$: (a) azimuthal component, (b) radial component and (c) vertical component. $\Delta u = \pm 0.001$, ——— positive, - - - - negative values.

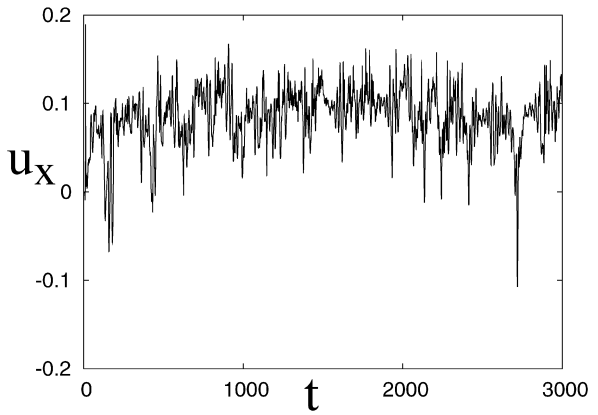

Fig. 15. Time history of pointwise samples of vertical velocity. $\Gamma = 0.5$, $Ra = 6.43 \times 10^6$ and $Pr = 5$, probe at $x/h = 0.25$ and $r/h = 0.2$.

$\Gamma = 1/2$ cell seems to switch direction from time to time. A closer look at the mean structure has revealed that the velocity switches are in fact temporary break-up of the single elongated cell into two counter-rotating rolls that in a short time disappear to reform a single cell with a different orientation with respect to the original one. This behaviour is a clear indicator of the instability of the mean flow in the $\Gamma = 1/2$ cell and this instability manifests itself at higher Rayleigh number with a flow bi-modality as recently observed by Roche et al. [11]. Since this flow bi-modality has not been observed in analogous experiments in water [12] it could be argued that the flow bi-modality might be related to the Prandtl number. Indeed in a preliminary simulation performed at $Pr = 5$ and $Ra = 6.43 \times 10^6$ (so that the Reynolds number $Re = \sqrt{Ra/Pr}$ in the first of Eq. (1) was the same as that of Fig. 7(b)) no velocity switches are observed (Fig. 15) thus indicating that the Prandtl number has a stabilizing effect on the mean flow. This aspect has been investigated in detail in a separate study and the interested reader is referred to Stringano and Verzicco [29].

Finally the effects on the flow dynamics of a background rotation, aligned with the gravity vector, has been investigated. In agreement with previous studies [14,32,19] it has been observed a slight increase of the heat transfer. This increase, however, is not a general feature but only occurs in a range of Rayleigh and Rossby numbers. It has been

shown, in fact, that the stability relation by Chandrasekar [13] can be rewritten in terms of Ro and Ra/Ra_C showing an explicit dependence in the Rayleigh number. Depending on Ra and Ro, therefore, the flow can be supercritical $Ra/Ra_C > 1$ or subcritical $Ra/Ra_C < 1$ and the Nusselt number can even drop to the purely conductive value $Nu = 1$. In the latter case, consistently with the Taylor–Proudman theorem, the rotation tends to inhibit the vertical motion and therefore the convective flow. This suppresses any flow motion and generates a purely vertical temperature gradient. This condition is highly desirable in solidification and crystal growth processes where the presence of horizontal temperature gradients induces material defects and crystal inhomogeneities.

Acknowledgement

This research has been performed with the financial support of CEMeC (Centro di Eccellenza di Meccanica Computazionale) of Politecnico di Bari and of the contract PRIN03.

References

[1] H. Bénard, Les turbillons cellulaires dans une nappe liquide, Revue Gen. Sci. Pures Appl. 11 (1990) 1261–1271.
[2] Lord Rayleigh, On convective currents in a horizontal layer of fluid when the higher temperature is on the under side, Philos. Mag. 32 (1916) 529–546.
[3] S. Grossmann, D. Lohse, Scaling in thermal convection: a unifying theory, J. Fluid Mech. 407 (2000) 27–56.
[4] L.N. Howard, Convection at high Rayleigh number, in: H. Görtler (Ed.), Proc. Eleventh Intl Congr. on Appl. Mech., Springer, 1966, pp. 1109–1115.
[5] R.H. Kraichnan, Turbulent thermal convection at arbitrary Prandtl number, Phys. Fluids 5 (11) (1962) 1374–1389.
[6] X. Chavanne, F. Chillà, B. Chabaud, B. Castaing, B. Hebral, Turbulent Rayleigh–Bénard convection in gaseous and liquid He, Phys. Fluids 13 (2001) 1300–1320.
[7] J.J. Niemela, L. Skrbek, R.R. Sreenivasan, R.J. Donnely, Turbulent convection at very high Rayleigh numbers, Nature 404 (2000) 837–841.
[8] R. Verzicco, R. Camussi, Numerical experiments on strongly turbulent thermal convection in a slender cylindrical cell, J. Fluid Mech. 477 (2003) 19–49.
[9] G. Amati, K. Koal, F. Massaioli, K.R. Sreenivasan, R. Verzieco, Turbulent thermal convection at high Rayleigh number for a Boussinesq fluid of constant Prandtl number, Phys. Fluids (2005), in press.
[10] X.Z. Wu, A. Libchaber, Scaling relations in thermal turbulence: The aspect-ratio dependence, Phys. Rev. A 45 (1992) 842–845.
[11] P.E. Roche, B. Castaing, B. Chabaud, B. Hebral, Prandtl and Rayleigh numbers dependences in Rayleigh–Bènard convection, Europhys. Lett. 58 (5) (2002) 693–698.
[12] C. Sun, H.D. Xi, K.Q. Xia, Azimuthal symmetry, flow dynamics and heat flux in turbulent thermal convection in a cylinder with aspect-ratio one-half, Phys. Rev. Lett. (2005), submitted for publication.
[13] S. Chandrasekar, Hydrodynamic and Hydromagnetic Stability, Oxford Univ. Press, 1961.
[14] H.T. Rossby, A study of Bénard convection with and without rotation, J. Fluid Mech. 36 (1969) 309–335.
[15] B. Boubnov, G.S. Golitsyn, Experimental study of convective structures in a rotating fluid, J. Fluid Mech. 167 (1986) 503–531.
[16] B. Boubnov, G.S. Golitsyn, Temperature and velocity field regimes of convective motions in a rotating fluid layer, J. Fluid Mech. 219 (1990) 215–239.
[17] S. Sakai, The horizontal scale of rotating convection in the geostrophic regime, J. Fluid Mech. 333 (1997) 85–95.
[18] P. Vorobieff, R. Ecke, Turbulent rotating convection: an experimental study, J. Fluid Mech. 458 (2002) 191–218.
[19] K. Julien, S. Legg, J. McWilliams, J. Werne, Rapidly rotating turbulent Rayleigh–Bénard convection, J. Fluid Mech. 322 (1996) 243–273.
[20] A. Belmonte, A. Tilgner, A. Libchaber, Temperature and velocity boundary layers in turbulent convection, Phys. Rev. E 50 (1) (1994) 269–279.
[21] G. Grötzbach, Spatial resolution requirements for direct numerical simulation of the Rayleigh–Bénard convection, J. Comput. Phys. 49 (1983) 241–264.
[22] R. Kerr, Rayleigh number scaling in numerical convection, J. Fluid Mech. 310 (1996) 139–179.
[23] R. Verzicco, R. Camussi, Transitional regimes of low-Prandtl thermal convection in a cylindrical cell, Phys. Fluids 9 (5) (1997) 1287–1295.
[24] G.S. Charlson, R.L. Sani, On thermoconvective instability in a bounded cylindrical fluid layer, Int. J. Heat Mass Transfer 14 (1971) 2157–2160.
[25] F.H. Busse, The oscillatory instability of convection rolls in a low Prandtl number fluid, J. Fluid Mech. 52 (1972) 97–112.
[26] R. Verzicco, R. Camussi, Prandtl number effects in convective turbulence, J. Fluid Mech. 383 (1999) 55–73.
[27] S. Cioni, S. Ciliberto, J. Sommeria, Strongly turbulent Rayleigh–Bénard convection in mercury: comparison with results at moderate Prandtl number, J. Fluid Mech. 335 (1997) 111–140.
[28] K.R. Sreenivasan, A. Bershadskii, J.J. Niemela, Mean wind and its reversals in thermal convection, Phys. Rev. E 65 (2002) 056306.
[29] G. Stringano, R. Verzicco, Mean flow structure in thermal convection in a cylindrical cell of aspect-ratio one half, J. Fluid Mech. (2005), in press.
[30] G.K. Batchelor, An Introduction to Fluid Mechanics, Cambridge Univ. Press, 1967.
[31] Z. Zhong, R. Ecke, V. Steinberg, Rotating Bénard convection: asymmetric modes and vortex states, J. Fluid Mech. 249 (1993) 135–159.
[32] Y. Liu, R. Ecke, Heat transport scaling in turbulent Rayleigh–Bénard convection: effects of rotation and Prandtl number, Phys. Rev. Lett. 79 (12) (1997) 2257–2260.
[33] K.M. Kim, A.F. Witt, H.C. Gatos, Crystal growth from the melt under destabilizing thermal gradients, J. Electrochem. Soc. 119 (1972) 1218–1226.